Mapana – Journal of Sciences
2026, Vol. 25, No. 2, *61 - 84*
ISSN 0975-3303 | https://doi.org/10.12723/mjs.77.4

Dipole Moments and Computational Study of 4(3IP)6MC and 4(3IP)6CLC Iodinated Coumarin Derivatives

Manjula Katageri*, Srinath†, Shivaleela B†, Sulochana Devar†, S. M. Hanagodimath†

Abstract

The spectroscopic properties of iodinated coumarin derivatives of 4(3-Iodophenoxymethl)-6-methyl-chromen-2one [4(3IP)6MT] and 6-chloro-4(3-Iodophynoxymethyl)-chromen-2one [4(3IP)6CLC] were compared experimentally. In pure organic solvents at room temperature, dipole moments (μ_g and μ_e) were evaluated using the solvatochromic shift method with Lippert, Bakshiev, and Kawski–Chamma–Viallet equations. The 4(3IP)6MC shows moderate ICT, largely influenced by hydrogen bonding in protic solvents; 4(3IP)6CLC demonstrates pronounced ICT even in nonpolar environments, suggesting stronger donor–acceptor interactions and a highly polar excited state. The change of dipole moments in 4(3IP)6CLC (4.9 D) is more than in 4(3IP)6MC (4.4 D). Further, the Kamlet-Taft and Catalán linear solvation energy relationship model was analyzed, revealing that in 4(3IP)6ClC, chlorine substitution enhances polarizability effects and reduces hydrogen-bonding contributions compared to 4(3IP)6MC with methyl substitution. In the theoretical computational study, (FMO, MEP and NLO) frontier molecular orbital, molecular electrostatic potential and nonlinear optical parameters were evaluated using the DFT/B3LYP/3-21G

* Govt. First Grade Residential SC/ST's Model College, Hadalageri, Tq. Muddebihal, Karnataka, India; manjulakatageri7@gmail.com

† Department of PG Studies and Research in Physics, Gulbarga University, Kalaburagi, Karnataka, India; srinathmore@gmail.com, shivaleelabphysics @gmail.com, sulochana.devar7@gmail.com, smhmath@rediffmail.com

level in Gaussian 16W. The results indicate enhanced NLO properties for 4(3IP)6ClC, suggesting its suitability as a promising material for advanced optical and imaging applications.

Keywords: Iodinated coumarin derivative, Solvatochromism, Dipole moment, Density functional theory (DFT), Nonlinear optical (NLO) properties.

1. Introduction

In the medical field, iodinated coumarin derivatives play a significant role in the treatment of human organs, as they contain a coumarin molecule with one or more iodine atoms attached. Iodinated coumarin derivatives are multifunctional compounds with significant applications in anticancer and antimycobacterial therapy, photodynamic therapy, fluorescence imaging, nonlinear optics, and radiopharmaceutical development, owing to the heavy-atom effect and the enhanced electronic properties imparted by iodine substitution. The iodine atom increases molecular size and enhances weak bond interactions, thereby enabling the diversity of enzymes and receptors in organisms. In anticancer agents, iodine increases lipophilicity and cell membrane permeability, enhances DNA intercalation, and inhibits enzymes. Due to iodine's properties, these coumarin derivatives are explored for medical imaging, cancer therapy (photodynamic/chemo), and as catalysts/probes [1-6]. Iodine acts as a strong electron-withdrawing substituent, enhancing NLO polarizability, first hyperpolarizability, and electrophilicity and showing strong intramolecular charge transfer (ICT). So, with specific iodine substitution, it enhances photophysical traits. The investigation of the photophysical characteristics of newly synthesised iodinated coumarin derivatives using various solvents in absorption and fluorescence spectra describes the dipole moment effect through the solvatochromic shift method [7]. In the current work, the solvatochromism of 4(3IP)6MC and 4(3IP)6CLC compounds has been examined using organic solvents with varying hydrogen-bonding properties and polarities. Experimentally, the dipole moments were evaluated with the Lippert [8], Bakshiev [9], and Kawaski-Chamma-Viallet [10-11] equations, together with the microscopic solvent polarity of Reichardt's parameters [12]. The solute-solvent interaction can also be described by Taft-Kamlet [13] and Catalan et al. [14] by the multiple regression method. The approach elucidates the influence of solvent hydrogen bonding and compares polarizability.

The computational analysis using Gaussian 16W software enables simulations ranging from small molecules to complex macromolecules. The

computational analyses were carried out using the DFT method on both iodinated molecules, 4(3IP)6MC and 4(3IP)6CLC, with the B3LYP/3-21 G basis set. The key molecular properties, FMO-frontier molecular orbitals, HOMO-LUMO, and MEP- the molecular electrostatic potential map, MEP and its contour map were studied with the optimised structure. The hyperpolarizability of first-order, the mean polarizability and dipole moment were calculated from nonlinear optical [NLO] properties [15, 16].

2. Resources and methods

Coumarin derivatives of iodinated molecules 4(3IP)6MC and 4(3IP)6CLC were procured from one of the authors as per the procedure reported in Ref. [17]. The molecular structures are presented in Figs. 1 and 2, respectively. The following spectroscopic-grade polar and nonpolar solvents were chosen from S.D. Fine Chemicals Limited: cyclohexane, 1,4-dioxane, toluene, diethyl ether, chloroform, ethyl acetate, tetrahydrofuran, butanol, propanol, acetone, ethanol, methanol, acetonitrile, dimethylformamide, dimethyl sulfoxide, and water, with an increase in their dielectric constant [18-21]. The low concentration of solute (1×10^{-5} M) has to be maintained in order to diminish the effects of self-absorption. A Model T90+ spectrometer (PG Instruments Ltd.) was used to gather UV-visible absorption spectra, and a Hitachi F7000 fluorescence spectrometer was used to record fluorescence spectra. The theoretical evaluation was carried out using Gaussian 16W software simulations. The presence of a heavy iodine atom in 4(3IP)6MC and 4(3IP)6CLC molecules, among all DFT methods, B3LYP in the 3-21G base set was executed for optimisation.

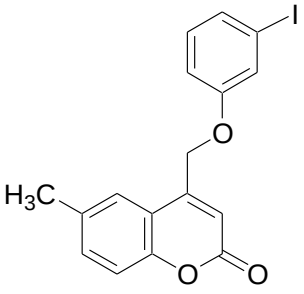

Figure 1: Structure of 4(3IP)6MC

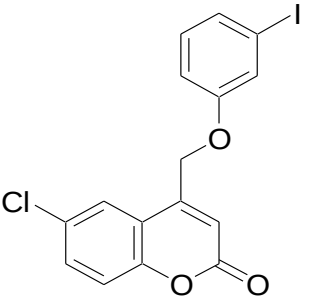

Figure 2: Structure of 4(3IP)6CLC

2.1 Solvatochromic shift method

The impact of a particular solute-solvent interaction on the spectroscopy of absorption and fluorescence of 4(3IP)6MC and 4(3IP)6CLC molecules was investigated experimentally using the solvatochromic shift method. Three

separate equations (1), (2), and (3) were used to determine the dipole moments [22].

Lippert's equation

$$\bar{\nu}_a - \bar{\nu}_f = m_1 F_1(\epsilon, n) + \text{constant} \quad (1)$$

Bakhshiev's equation

$$\bar{\nu}_a - \bar{\nu}_f = m_2 F_2(\epsilon, n) + \text{constant} \quad (2)$$

Kawaski-Chamma-Viallet's equation

$$\frac{\bar{\nu}_a + \bar{\nu}_f}{2} = m_3 F_3(\epsilon, n) + \text{constant} \quad (3)$$

where the absorption maxima are denoted with $\overline{\nu_a}$ (cm^{-1}) and fluorescence maxima are denoted by $\overline{\nu_f}$ (cm^{-1}). The solvents refractive index is 'n', and the dielectric constant is 'ϵ', and the polarity function parameters of the three different equations, Lippert, Bakhshiev and Kawaski-Chamma-Viallet are symbolized as $F_1(\epsilon, n)$, $F_2(\epsilon, n)$ and $F_3(\epsilon, n)$, having equations (4),(5) and (6) respectively [23].

$$F_1(\epsilon, n) = \left[\frac{\epsilon-1}{2\epsilon-1} - \frac{n^2-1}{2n^2+1}\right] \quad (4)$$

$$F_2(\epsilon, n) = \left[\frac{\epsilon-1}{\epsilon+2} - \frac{n^2-1}{n^2+2}\right]\frac{(2n^2+1)}{(n^2+2)} \quad (5)$$

$$F_3(\epsilon, n) = \frac{(2n^2+1)}{2(n^2+2)}\left[\frac{\epsilon-1}{\epsilon+2} - \frac{n^2-1}{n^2+2}\right] + \frac{3(n^4-1)}{2(n^2+2)^2} \quad (6)$$

From linear graphs of $(\overline{\nu_a} - \overline{\nu_f})$ against $F_1(\epsilon, n)$, $(\overline{\nu_a} - \overline{\nu_f})$ against $F_2(\epsilon, n)$ and $(\overline{\nu_a} + \overline{\nu_f})/2$ against $F_3(\epsilon, n)$ gives slopes m_1, m_2, and m_3 from equations (1), (2), and (3), respectively. They are enumerated in Eqns. (7), (8) and (9).

$$m_1 = \frac{2(\mu_e - \mu_g)^2}{hca^3} \quad (7)$$

$$m_2 = \frac{2(\mu_e - \mu_g)^2}{hca^3} \quad (8)$$

$$m_3 = \frac{2(\mu_e^2 - \mu_g^2)}{hca^3} \quad (9)$$

where μ_g and μ_e are ground- and excited-state dipole moments. The Planck constant is h, and the light velocity is c. The radius of the Onsager's cavity of molecule, "a," was calculated using J.T. Edward's [24] atomic increment method. There is a tiny angle ϕ between the μ_e and μ_g when they are not collinear. Equation (10) below can be used to estimate this angle.

$$\cos\Phi = \frac{1}{2\mu_g\mu_e}\left[\left(\mu_g^2 + \mu_e^2\right) - \frac{m_2}{m_3}\left(\mu_e^2 - \mu_g^2\right)\right] \quad (10)$$

Assuming μ_e and μ_g are almost aligned with one another, which provides the Eqns. (11) and (12).

$$\mu_g = \frac{m_3 - m_2}{2}\left[\frac{hca^3}{2m_2}\right]^{1/2} \quad \text{For } (m_3 > m_2) \tag{11}$$

$$\mu_e = \frac{m_3 + m_2}{2}\left[\frac{hca^3}{2m_2}\right]^{1/2} \tag{12}$$

Reichardt correlated the microscopic polarity parameter E_T^N with Stokes shift, which was later refined by Ravi *et al.* [25]. The change in dipole moment was evaluated using equation (13).

$$\overline{\nu_a} - \overline{\nu_f} = 11307.6 \times E_T^N \left[\left(\frac{\Delta\mu}{\Delta\mu_B}\right)^2 \left(\frac{a_B}{a}\right)^2\right] + \text{constant} \tag{13}$$

The quantities 'a' and $\Delta\mu$ of present interest molecules 4(3IP)6MC and 4(3IP)6CLC are Onsager's cavity radius and change of dipole moment. The comparative Betadine dye has $a_B = 6.2$Å and $\Delta\mu_B$=9D and the value of E_T^N is given by Eqn. (14).

$$E_T^N = \frac{E_T(Solvent) - 30.7}{32.4} \tag{14}$$

The E_T(Solvent) The solvatochromic Betadine dye, pyridinium N-phenolate, is estimated with the respective maximum absorbing wavelength (λ_{max}) determined from Eqn. (15) [26].

$$E_T(Solvent) = 28.591 / (\lambda_{max}) \tag{15}$$

2.2. Kamlet-Taft and Catalan method:

The molecule's spectral characteristics were correlated with solvent interactions with the solute using the Kamlet-Taft and Catalan models via a linear multiple regression. According to Eq. (16), the Kamlet formalism solvent effects are described by the polarizability parameter (π*), which accounts for charge stabilisation via nonspecific dielectric interactions, along with the hydrogen bond donor strength (α) and the hydrogen bond acceptor strength (β) [27,28].

$$y = y_0 + a\alpha + b\beta + c\pi^* \tag{16}$$

Here y_0 and y represent the relevant spectral property in solution and gas. The HBD, HBA, and dielectric interaction coefficients are 'a', 'b' and 'c' respectively.

Catalan Eqn. (17) extends this analysis by employing four empirical solvent parameters: acidity (SA), basicity (SB), polarizability (SP) and dipolarity (SdP) with corresponding regression values a_{SA} , b_{SB}, c_{SP} and d_{SdP}.

$$y = y_0 + a_{SA}\ SA + b_{SB}\,SB + c_{SP}\,SP + d_{SdP}\,SdP \quad (17)$$

The variables y and y_0 retain their usual meanings. This equation helps separate and quantify different solvent effects on spectral behaviour.

2.3. Computational Study

2.3.1. Frontier Molecular Orbital (FMO)

The compounds reactivity, stability, and interaction properties were evaluated using frontier molecular orbital energies. These include LUMO, the lowest unoccupied molecular orbital, which has a strong electrophilic nature and functions as an electron acceptor, whereas HOMO, the highest occupied molecular orbital, is a strong nucleophile and an electron donor. HOMO and LUMO energies with ionisation potential (z) and electron affinity (e) are used to characterise the behaviour of a pair of electrons inside a molecule. There are comparable equations for the parameters of global reactivity of chemical descriptors such as electronegativity (χ), potential (μ), hardness (η), softness (σ), and electrophilicity index (ω)[29-31].

$\chi = (½)\ (z+e)$	$\mu = -(½)\ (z+e)$	$\eta = (½)\ (z-e)$	$\sigma = (½)\ (1/\eta)$	$\omega = (½)\ (\mu^2/\eta)$

A measure of molecule stability is the energy band gap in between the HOMO-LUMO orbitals. A narrower band gap increases reactivity and promotes electron transport, while a larger gap increases stability and decreases chemical reactivity. Intramolecular charge transfer between electron-donating and electron-accepting groups via π-conjugated pathways results in HOMO–LUMO separation. The average tendency of a molecule to attract electrons is represented by (χ), whilst the tendency of electrons to escape from the molecule at equilibrium is reflected by (μ). The (η) and (σ) are inversely related and offer insight into resistance toward charge transfer. The (ω) measures the capability of a molecule to accept electrons.

2.3.2. Non-linear optical properties

The materials respond nonlinearly to the charge distribution polarization induced by the interaction of a substance with electromagnetic radiation. Nonlinear properties play a vital role in optical modulation in telecommunications, dynamic image processing, signal processing, and optical interconnections. The responsibility for NLO features lies in the delocalisation of electrons in organic molecules, which increases polarizability and enhances hyperpolarizability. The electric dipole moment (μ), polarizability (α), and first- and second-order hyperpolarizabilities (β and γ) of an isolated molecule subjected to an

external electric field determine its NLO characteristics response [28–30]. The Taylor series expansion provides the total electric dipole moment (μ_{tot}), the polarizability in static (α_0), the anisotropy of polarizabilities ($\Delta\alpha$), and the hyperpolarizability in static of first-order (β_0), which are extracted and presented in Equations (18) to (21)[32].

$$\mu = \sqrt{\mu_x^2 + \mu_y^2 + \mu_z^2} \tag{18}$$

$$\alpha_o = \frac{[\alpha_{xx}+\alpha_{yy}+\alpha_{zz}]}{3} \tag{19}$$

$$\Delta\alpha = \sqrt{\frac{[\alpha_{xx}-\alpha_{yy}]^2+[\alpha_{yy}-\alpha_{zz}]^2+[\alpha_{zz}-\alpha_{xx}]^2+6\alpha_{xz}^2}{2}} \tag{20}$$

$$\beta_o = \sqrt{[\,\beta_{xxx} + \beta_{xyy} + \beta_{xzz}\,]^2 + [\,\beta_{yyy} + \beta_{yxx} + \beta_{yzz}\,]^2 + [\,\beta_{zzz} + \beta_{zxx} + \beta_{zyy}\,]^2} \tag{21}$$

3. Results and Discussion

3.3.1. Solvatochromic Dipole moment

The spectroscopic behaviour of the iodinated coumarin derivatives, 4(3IP)6MC and 4(3IP)6CLC, is illustrated through normalised absorption spectra in Figs. 3a and 4a and fluorescence spectra in Figs. 3b and 4b using polar and nonpolar solvents, respectively. Tables 1 and 2 summarise the corresponding absorption and emission maxima wavelengths, wave numbers, Stokes shifts, and arithmetic mean values for 4(3IP)6MC and 4(3IP)6CLC, respectively. The solvent polarity functions $F_1(\varepsilon,n)$, $F_2(\varepsilon,n)$, and $F_3(\varepsilon,n)$ and E_T^N for the respective solvents are embedded in Table 3.

The positive solvatochromic behaviour was observed in both molecules. An increase in Stokes shift is observed with increasing solvent polarity, indicating enhanced intramolecular charge transfer and a corresponding bathochromic (red) shift. For the 4(3IP)6MC, the Stokes shift is 763 cm^{-1} in nonpolar toluene, increases to 7241 cm^{-1} in the polar protic solvent methanol, and reaches 9914 cm^{-1} in the aprotic solvent ethyl acetate. A large Stokes shift (strong ICT) was observed in ethyl acetate, ethanol, water, and methanol. A moderate Stokes shift (moderate ICT) was observed in DMSO, DMF, THF, propanol, cyclohexane, and acetone. Low Stokes shift (weak ICT) in chloroform, toluene, and acetonitrile. In the case of 4(3IP)6CLC, the minimum Stokes shift of 1191 cm^{-1} was observed in acetone, while the maximum of 13957 cm^{-1} occurs in protic butanol. A large Stokes shift (strong ICT) was observed in butanol, diethyl ether, and water; a significant

Stokes shift (large ICT) was observed in DMSO, DMF, propanol, cyclohexane, ethanol, and acetonitrile. Low Stokes shift (weak ICT) in toluene and acetonitrile. By comparing both molecules, 4(3IP)6MC has a general Stokes shift range of 700-10000 cm^{-1}, and 4(3IP)6CLC has a very broad range of ~14000 cm^{-1}. Hence, 4(3IP)6CLC exhibits a larger Stokes shift and stronger solvent dependence than 4(3IP)6MC, indicating more efficient intramolecular charge transfer (ICT). While 4(3IP)6MC shows moderate ICT, largely influenced by hydrogen bonding in protic solvents, 4(3IP)6CLC demonstrates pronounced ICT even in nonpolar environments, suggesting stronger donor–acceptor interactions and a highly polar excited state.

For 4(3IP)6MC, Figs. 5(a), 5(b) & 5(d) represent the increment of Stokes shift with polarity functions F_1, F_2, and E_T^N, and the decrement of the average value of wave numbers with F_3 is shown in Fig. 5(c). For 4(3IP)6CLC, Figs. 6(a), 6(b), & 6(d) and 6(c) show the similar staging with solvent polarity functions. The statistical treatment and dipole moments with the Onsager radius are displayed in Table 4. The 4(3IP)6MC has a μ_g of 2.8 Debye (D) and μ_e of 7.2 D. The Lippert, Bakhshiev, and Kawasaki-Chamma-Viallet equations have μ_e of 11.3D, 7.2D, and 7.2D, respectively. The change of dipole moment is 4.4 D, and from E_T^N it is 3.21D. Where the 4(3IP)6CLC has a dipole moment of μ_g=1.9 D and μ_e=6.7 D. From the equations (4), (5), and (6), we have 9.8D, 6.7D, and 6.7D, respectively. The change of dipole moment is 4.9D and 3.4D from E_T^N. The ratio of dipole moments (μ_e/μ_g) of 4(3IP)6MC is 2.57, and for 4(3 IP)6CLC, it is 3.52.

The 4(3IP)6MC exhibits a higher ground state dipole moment due to the electron-donating methyl group compared to the electron-withdrawing chlorine group of 4(3IP)6CLC. The dipole moment upon excitation change ($\Delta\mu$) is found to be greater for 4(3IP)6CLC (4.9 D) compared to 4(3IP)6MC, is (4.4D). This can be attributed to the electron-withdrawing nature of the chlorine substituent, which results in a relatively less polarized ground state but undergoes significant charge redistribution in the excited state. Consequently, 4(3IP)6CLC experiences a larger increase in dipole moment upon excitation, indicating stronger excited-state intramolecular charge transfer and enhanced sensitivity to solvent polarity. Thereupon, it confirms that 4(3IP)6CLC has a superior fluorescence character compared to 4(3IP)6MC experimentally [33-38].

The theoretical computational value of μ_g for 4(3IP)6MC is 6.47 D, and for 4(3IP)6CLC, it is 4.13 D. This is a discernible gap between the ground-state dipole moment's computational and experimental values. Experimentally, the solvent interactions and atmospheric influences are responsible for the observed discrepancy.

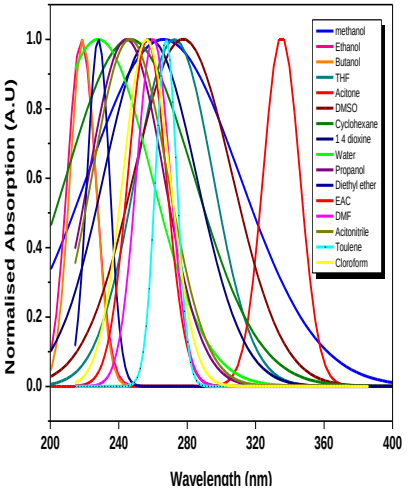

Figure 3(a): 4(3IP)6MC- Absorption spectra spectra

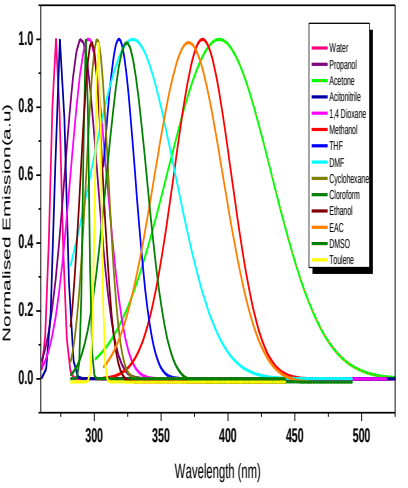

Figure 3(b): 4(3IP)6MC- Emission

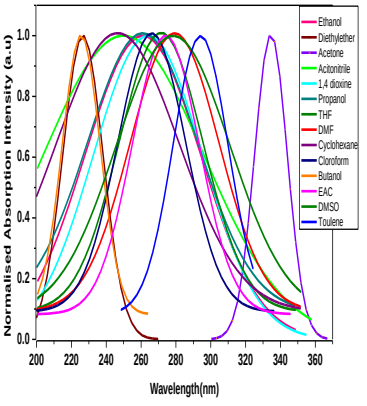

Figure 4(a): 4(3IP)6CLC- Absorption Spectra

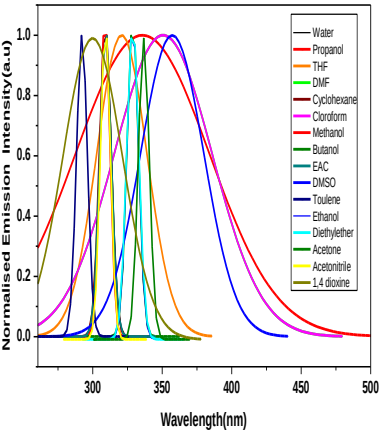

Figure 4(b): 4(3IP)6CLC- Emission spectra

Table 1: Spectral specifications of 4(3IP)6MC

Solvents	λ_a **nm**	λ_f **nm**	$\overline{\nu_a}$ **cm^{-1}**	$\overline{\nu_f}$ **cm^{-1}**	$(\overline{\nu_a} - \overline{\nu_f})$ **cm^{-1}**	$(\overline{\nu_a} + \overline{\nu_f})/2$ **cm^{-1}**
Water	225	271	44503	36854	7649	40679
Dimethyl sulfoxide	276	329	36215	30406	5808	33310
Dimethylformamide	279	336	35809	29788	6022	32798
Acetonitrile	258	274	38763	36470	2293	37616

Methanol	321	418	31153	23911	7241	27532
Ethanol	230	287	43478	34892	8586	39185
Acetone	337	394	29706	25386	4319	27546
Propanol	252	289	39695	34602	5093	37149
Butanol	270	300	37037	33333	3704	35185
Tetrahydrofuran	273	318	36616	31486	5130	34051
Ethyl acetate	288	403	34722	24808	9914	29765
Chloroform	268	278	37313	35958	1355	36636
Diethyl ether	268	300	37313	33333	3980	35323
Toluene	288	294	34722	33959	763	34341
1,4-Dioxane	258	294	38763	33967	4796	36365
Cyclohexane	246	292	40670	34270	6400	37470

Table 2: Spectral specifications of 4(3IP)6CLC

Solvents	**λ_a nm**	**λ_f nm**	**$\overline{\nu_a}$ cm^{-1}**	**$\overline{\nu_f}$ cm^{-1}**	**$(\overline{\nu_a} - \overline{\nu_f})$ cm^{-1}**	**$(\overline{\nu_a} + \overline{\nu_f})/2$ cm^{-1}**
Water	228	310	43860	32258	11602	38059
Dimethyl sulfoxide	280	357	35714	28011	7703	31863
Dimethylformamide	279	352	35842	28409	7433	32126
Acetonitrile	250	310	40000	32258	7742	36129
Methanol	264	311	37879	32154	5724	35017
Ethanol	261	328	38314	30488	7826	34401
Acetone	334	337	30864	29674	1191	30269
Propanol	260	336	38462	29762	8700	34112
Butanol	225	328	44444	30488	13957	37466
Tetrahydrofuran	270	322	37037	31056	5981	34046
Ethyl acetate	273	310	36630	32258	4372	34444
Chloroform	267	352	37453	33223	4231	35338
Diethyl ether	228	328	43860	30488	13372	37174
Toluene	287	299	34843	32154	2689	33499
1,4-Dioxane	264	301	37879	33445	4434	35662
Cyclohexane	246	311	40650	32258	8392	36454

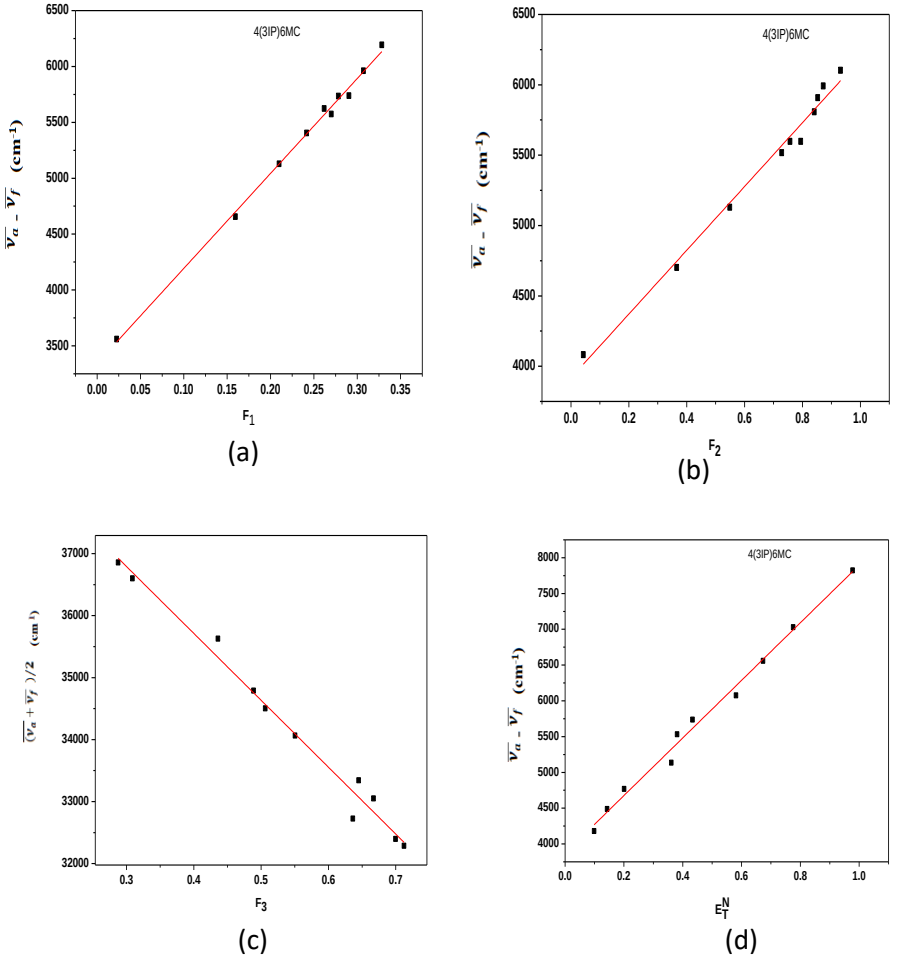

Figure 5: The Stokes shift with (a) Lippert (b) Bakhshiev (d) Microscopic Solvent polarity functions and (c) Arithmetic mean with Kawski-chamma-Vaillet polarity function of 4(3IP)6MC.

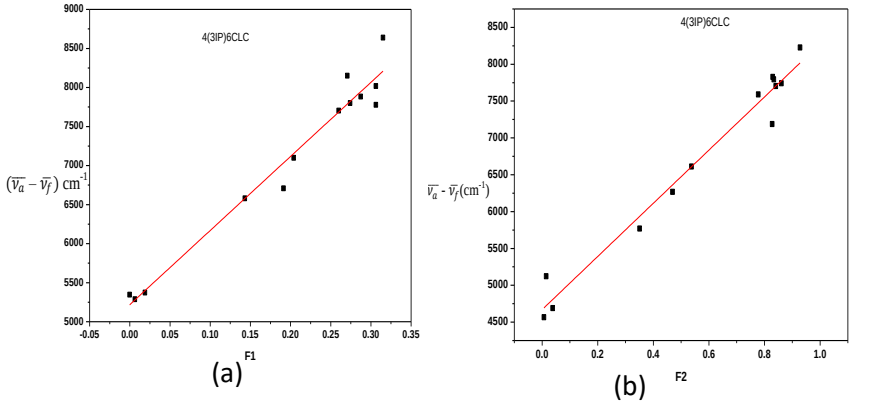

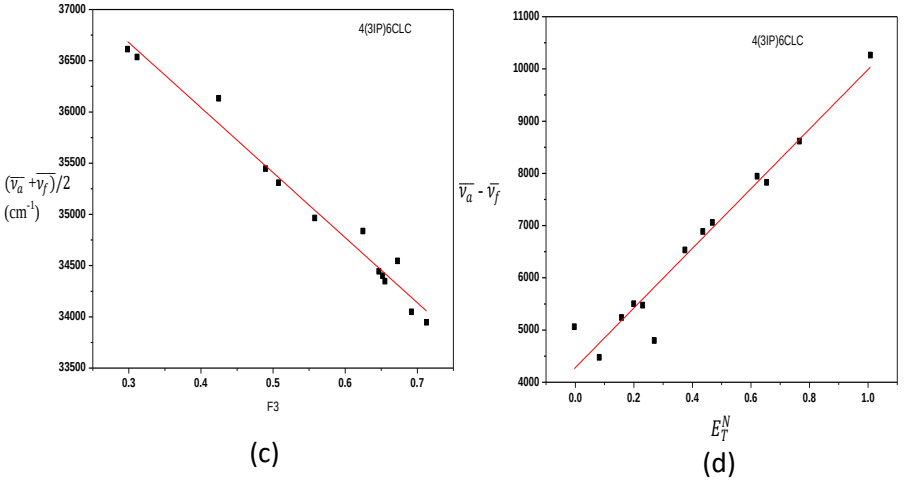

Figure 6: The Stokes shift with **(a)** Lippert **(b)** Bakhshiev **(d)** Microscopic solvent polarity functions and **(c)** Arithmetic mean with Kawski-chamma-Vaillet polarity function of 4(3IP)6CLC.

Table 3: Solvent polarity functional specifications

Solvents	**ε**	**n**	**F_1 (ε,n)**	**F_2 (ε,n)**	**F_3 (ε,n)**	**E_T^N**
Water	80.0	1.333	0.320	0.914	0.684	1
Dimethyl sulfoxide	47.0	1.479	0.260	0.841	0.699	0.44
Dimethylformamide	38.2	1.430	0.275	0.839	0.711	0.386
Acetonitrile	36.6	1.344	0.305	0.861	0.665	0.460
Methanol	32.7	1.329	0.308	0.855	0.652	0.762
Ethanol	24.6	1.361	0.289	0.830	0.652	0.654
Acetone	20.7	1.359	0.284	0.790	0.640	0.355
Propanol	20.6	1.385	0.274	0.781	0.653	0.617
Butanol	17.4	1.399	0.263	0.749	0.646	0.586
Tetrahydrofuran	7.58	1.407	0.210	0.549	0.551	0.207
Ethyl acetate	6.08	1.372	0.201	0.493	0.499	0.228
Chloroform	4.81	1.446	0.148	0.371	0.494	0.259
Diethyl ether	4.26	1.353	0.164	0.370	0.439	0.117
Toluene	2.38	1.497	0.013	0.029	0.035	0.099

Solvents	**ε**	**n**	**F_1 (ε,n)**	**F_2 (ε,n)**	**F_3 (ε,n)**	**E_T^N**
1,4-Dioxane	2.22	1.422	0.022	0.044	0.308	0.164
Cyclohexane	2.02	1.426	0.001	0.002	0.289	0.006

Table 4: Statistical treatment of 4(3IP)6MC and 4(3IP)6CLC with dipole moments

Coumarin	Onsager Radius a (Å)	Statistical relations			μ-Dipole Moments								
		Slope (cm^{-1})	R square	n	μ_g^a (D)	μ_g^b (D)	μ_e^c (D)	μ_e^d (D)	μ_e^e (D)	μ_e^f (D)	$\Delta\mu^g$ (D)	$\Delta\mu^h$ (D)	$\left(\frac{\mu_e}{\mu_g}\right)^j$
4(3IP)6MC	4.40	m_1 =8497	0.9958	10	6.47	2.8	7.2	11.3	7.2	7.2	4.4	3.21	2.57
		m_2= 2267	0.9862	10									
		m_3= -5137	0.9653	11									
		m= 4025	0.9031	10									
4(3IP)6CLC	4.05	m_1 = 9489	0.9604	13	4.13	1.9	6.7	9.8	6.7	6.7	4.9	3.4	3.52
		m_2= 3608	0.9703	13									
		m_3= -6346	0.9750	13									
		m= 5710	0.9410	13									

Where, 1D = 3.34×10^{-30}cm = 10^{-18}esu.cm, R^2 is the correlation coefficient and 'n' is the number of points.

Ground state dipole moments: μ_g^a from DFT optimization geometry, μ_g^b is calculated from Eqn. (11).

Excited state dipole moments evaluated: μ_e^c is from Eqn. (12), μ_e^d is from Lippert's Eqn. (7), μ_e^e is from Bakhshiev's Eqn. (8), μ_e^f is from Kawaski-Chamma-Viallet's Eqn. (9).

Change of dipole moment evaluated: $\Delta\mu^g$ is from Eqns. (11) and (12), $\Delta\mu^h$ is from Eqn. (14).

$[\mu_e/\mu_g]^j$ is the ratio of dipole moment.

3.2. Parameters of Kamlet-Taft and Catalan equations

A quantitative evaluation of solvent interactions influencing on the spectra of absorption and fluorescence of 4(3IP)6MC and 4(3IP)6CLC was carried out by the equations of Kamlet-Taft and Catalan through the multiple regression approach. The corresponding relationships are expressed from Eqs. (22) to (25). The solvent parameters (α), (β), (π*), (SA), (SB), (SP), and (SdP) are listed in Table 5 [39, 40].

Kamlet-Taft equations of 4(3IP)6MC

$\overline{\nu_a}$ (cm^{-1}) = 28944 -164 α +5570 β + 9399 π* r = 0.9865

$\bar{\nu}_f$ (cm^{-1}) = 23268 -3280 α +19627 β - 350 π* r = 0.9845 (22)

$\overline{\Delta\nu}$ (cm^{-1}) = 346+338 α +6250 β +2736 π* r = 0.9915

Kamlet-Taft equations of (4(3IP)6CLC

$\bar{\nu}_a$ (cm^{-1}) = 31125 +1240 α +2457 β + 9376 π* r = 0.9821

$\bar{\nu}_f$ (cm^{-1}) = 27969 -501α +5515 β +1014 π* r = 0.9511 (23)

$\overline{\Delta\nu}$ (cm^{-1}) = 358+1222 α +4761β +6842 π* r = 0.9931

It is observed from Eqn. (22) that in 4(3IP)6MC the HBA parameter has more influence on fluorescence and stokes shift. The dielectric (π*) of the solvent and the HBD parameter cannot be ignored. From Eqn. (23), it is evident that the dielectric (π*) interactions have a significant effect on the 4(3IP)6CLC, and the contributions of HBA is more than the HBD parameter [40] and it shows greater contribution from dipolarity/polarizability (π*), highlighting the role of dielectric stabilization.

Catalan equations of 4(3IP)6MC

$\bar{\nu}_a$ (cm^{-1}) = 40903 + 6700 SA + 4431 SB -23580 SP + 12634 SdP r = 0.9894

$\bar{\nu}_f$ (cm^{-1}) = 17007 - 2734 SA +16313 SB +10217 SP + 857 SdP r = 0.9864 (24)

$\overline{\Delta\nu}$ (cm^{-1}) = - 2891 + 1937 SA +4938 SB +4799 SP +2675 SdP r = 0.9953

Catalan equations of (4(3IP)6CLC

$\bar{\nu}_a$ (cm^{-1}) = 23154 + 3080 SA + 1986 SB +12496 SP + 6604 SdP r=0.9474

$\bar{\nu}_f$ (cm^{-1}) = 22676 - 552 SA + 3291 SB +7880 SP + 1994 SdP r=0.9685 (25)

$\overline{\Delta\nu}$ (cm^{-1}) = -3824 + 3963 SA +5515 SB +7142 SP +3559 SdP r=0.9623

From Eqns. (24) and (25), Catalán analysis reveals that for 4(3IP)6MC, absorption is mainly controlled by solvent polarizability, while fluorescence is dominated by hydrogen-bonding interactions (SB). For 4(3IP)6CLC, polarizability (SP) dominates both absorption and fluorescence, indicating predominantly nonspecific interactions. Overall, chlorine substitution enhances polarizability effects and reduces hydrogen-bonding contributions compared to the methyl derivative.

Table 5: Solvatochromic Kamlet and Catalan empirical solvent scale parameters [40].

Solvents	**α**	**β**	**Π***	**SA**	**SB**	**SP**	**SdP**
Water	1.170	0.470	1.090	1.062	0.025	0.681	0.997
Dimethyl sulfoxide	0.000	0.760	1.000	0.072	0.647	0.830	1.000
Dimethylformamide	0.000	0.690	0.880	0.000	0.475	0.651	0.907
Acetonitrile	0.190	0.310	0.750	0.044	0.286	0.645	0.974
Methanol	0.980	0.660	0.600	0.605	0.545	0.608	0.904
Ethanol	0.860	0.750	0.540	0.400	0.658	0.633	0.783
Acetone	0.080	0.480	0.710	0.031	0.613	0.759	0.977
Propanol	0.840	0.900	0.520	0.367	0.782	0.658	0.748
Butanol	0.840	0.840	0.470	0.341	0.809	0.674	0.655
Tetrahydrofuran	0.000	0.550	0.580	0.000	0.591	0.714	0.634
Ethyl acetate	0.000	0.450	0.550	0.000	0.542	0.656	0.603
Chloroform	0.200	0.100	0.530	0.047	0.071	0.783	0.786
Diethyl ether	0.000	0.490	0.270	0.000	0.562	0.616	0.694
Toluene	0.000	0.110	0.540	0.000	0.128	0.782	0.284
1,4-Dioxane	0.000	0.370	0.550	0.000	0.444	0.717	0.312
Cyclohexane	0.000	0.000	0.000	0.000	0.482	0.766	0.745

3.3. Computational Analysis

3.3.1.FMO and MEP

The molecular geometries of 4(3IP)6MC and 4(3IP)6CLC were optimized using the Gaussian 16W software, employing the DFT/B3LYP in the 3-21G base set. The optimized structure, along with the direction of the dipole moment, is illustrated in Figs. 7(a) and 7(b). The computational value of μ_g, was 6.47 D for 4(3IP)6MC and 4.13 D for 4(3IP)6ClC.

The frontier molecular orbital (FMO) surfaces of HOMO and LUMO are computed in the gas phase depicted in Figs. 8(a) and 8(b) for 4(3IP)6MC and in Figs. 9(a) and 9(b) for 4(3IP)6CLC. The chemical quantities are listed in Table 5. Based on HOMO-LUMO energy, the ionization potential and electron affinity of 4(3IP)6MC are 0.2338 eV and 0.0741 eV, and for 4(3IP)6CLC, they are 0.2410 eV and 0.0839 eV, respectively. The HOMO-

LUMO band gap of 4(3IP)6MC is marginally higher by 0.0026 eV compared to 4(3IP)6CLC. The chemical softnesses are 6.2617 eV and 6.3645 eV for the respective molecules, which signifies that 4(3IP)6CLC is relatively softer and more polarizable than 4(3IP)6MC. In addition, electronegativity and chemical potential 4(3IP)6CLC are higher, revealing a more uneven electron density distribution and a greater tendency for electrons to escape from the equilibrium system. Also, the electrophilicity index further clarifies that the electron-accepting capability of 4(3IP)6CLC is approximately 0.02 eV higher than that of 4(3IP)6MC. In total, 4(3IP)6CLC exhibits stronger ICT characteristics, enhanced electron-accepting ability, and is more stabilised in an excited state.

Molecular electrostatic potential (MEP) analysis provides insight into the electron density distribution, identifying electron-rich (Electrophilic) and electron-deficient regions (nucleophilic) responsible for solute–solvent interactions. These regions govern hydrogen bonding and polarity effects observed in spectroscopic properties. The MEP maps and their contours of 4(3IP)6MC were visualized in Figs. 10(a) and 10(b), and for 4(3IP)6CLC, they were in Figs. 11(a) and 11(b). The spreading of charges is visualised with various colors. The strong blue nucleophile region on the donor indicates the most positive electrostatic potential, which is prone to electrophilic attack, whereas the strong red electrophilic region on the acceptor shows the most negative electrostatic potential, favouring nucleophilic attack. For 4(3IP)6MC the electrostatic potential ranges from −6.455 a.u. (red) to +6.455 a.u. (blue). Similarly, the 4(3IP)6CLC molecule exhibits potential extrema at −5.886 a.u. (red) and +5.886 a.u. (blue). The negative electrostatic potential is mainly localised around the oxygen atom bonded to the carbon atom, highlighting this site as highly susceptible to electrophilic attack. Conversely, the iodine (I) and hydrogen (H) atoms attached to the benzene ring exhibit positive electrostatic potentials, which are favourable for nucleophilic attack. The variation in electrostatic potential is represented by colours, with increasing potential values following the order: red < orange < yellow < green < blue. In an MEP contour map, closely spaced contours indicate a strong potential gradient and high polarity, and widely spaced contours indicate low polarity and less reactive regions [41, 42].

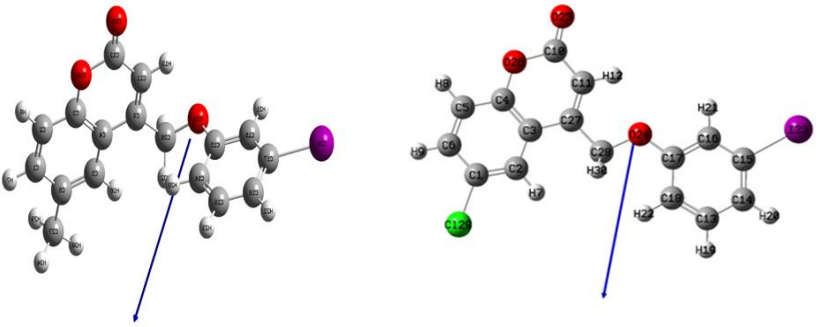

(a) 4(3IP)6MC (b) 4(3IP)6CLC

Figure 7: Optimized structure with dipole moment vector

Table 6: FMO parameters in gas phase.

Parameter (in eV)	**4(3IP)6MC**	**4(3IP)6CLC**
E_{HOMO}	-0.2338	-0.2410
E_{LUMO}	-0.0741	-0.0839
ΔE-Energy gap	0.1597	0.1571
Z-Ionization potential	0.2338	0.2410
E-Electron affinity	0.0741	0.0839
χ -Electro negativity	0.1539	0.1625
μ- Chemical potential	-0.1539	-0.1625
Ƞ- Chemical hardness	0.0798	0.0785
σ-Chemical softness	6.2617	6.3645
ω-Electrophilicity	0.1484	0.1680

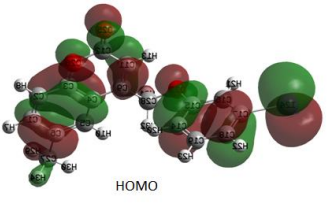

Figure 8(a): HOMO [4(3IP)6MC]

Gas Phase

E_{LUMO} = **-0.0741 eV**

ΔE = **-0.1597 eV**

E_{HOMO} = -0.2338 eV

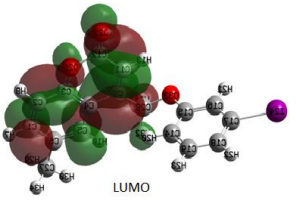

Figure 8(b): LUMO [4(3IP)6MC]

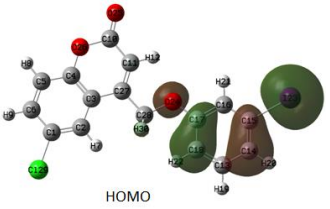

Gas Phase

E_{LUMO} = **-0.0839 eV**

ΔE = **-0.1571eV**

E_{HOMO} **= -0.2410eV**

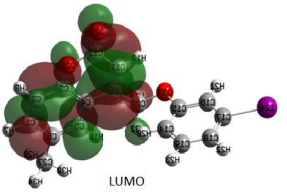

Figure 9(a): HOMO [4(3IP)6CLC]

Figure 9(b): LUMO [4(3IP)6CLC]

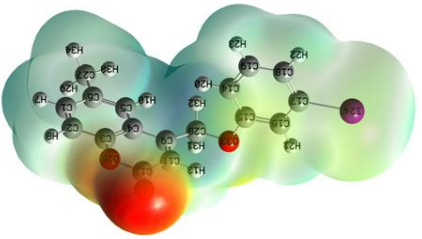

Figure 10(a): [4(3IP)6MC] MEP map

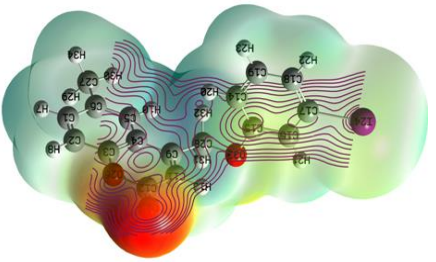

Figure 10(b): [4(3IP)6MC] MEP Contour map

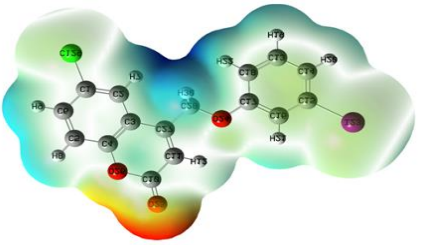

Figure 11(a): 4(3IP)6CLC MEP map

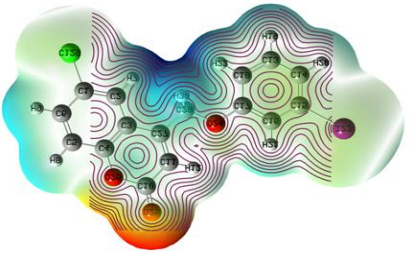

Figure 11(b): 4(3IP)6CLC MEP Contour map

3.3.2. Nonlinear optical (NLO) properties

The NLO parameters of 4(3IP)6MC and 4(3IP)6CLC were computed and compared with urea NLO properties determined by DFT/B3LYP/3-21 technique, and the results are summarised in Table 7. The key results include a total dipole moment (μ_{tot}) of 6.471D for 4(3IP)6MC and 4.129D for 4(3IP)6CLC, both of which exceed the value of the standard NLO reference urea (3.9 D). The molecular polarizability (α_0) for 4(3IP)6MC is 29.317×10^{-24} esu, and for 4(3IP)6CLC is 29.274×10^{-24} esu., whereas urea: 3.749×10^{-24} esu.

The hyperpolarizability of first-order (β0) for 4(3IP)6MC is 1.84 × 10^{-30} esu, and 4(3IP)6CLC has 12.083 ×10^{-30} esu and urea has 0.3728×10^{-30} esu. A comparative analysis with urea, both molecules exhibit significantly enhanced NLO responses. Notably, the first-order hyperpolarizability of 4(3IP)6CLC is nearly 30 times more than that of urea [43,44]. This indicates a strong response to external electric fields, highlighting its potential as an efficient nonlinear optical material for advanced imaging applications.

Table 7: NLO properties of 4(3IP)6MC and 4(3IP)6CLC in DFT/B3LYP

μ	Electric Dipole Moment (Debye)		α	Polarizability (10^{-24}) esu		β	First order hyper polarizabilty (10^{-30}) esu	
	4(3IP)6MC	4(3IP)6CLC		4(3IP)6MC	4(3IP)6CLC		4(3IP)6MC	4(3IP)6CLC
μ_x	-5.667	1.391	α_{xx}	28.207	23.754	β_{xxx}	-0.521	0.286
μ_y	-1.245	-3.835	α_{xy}	10.166	2.027	β_{yxx}	0.420	-2.747
μ_z	-2.864	-0.636	α_{yy}	39.108	42.289	β_{xyy}	-0.251	-0.129
μ_{tot}	**6.471**	**4.129**	α_{xz}	40.716	-13.780	β_{yyy}	0.216	-0.163
			α_{yz}	0.681	-7.057	β_{zxx}	-0.145	-0.255
			α_{zz}	20.637	21.779	β_{xyz}	-0.158	-0.147
			α_0	**29.317**	**29.274**	β_{zyy}	1.562	0.072
			Δα	**72.330**	**30.883**	β_{xzz}	-0.469	0.277
						β_{yzz}	0.125	-9.161
						β_{zzz}	-0.292	-0.157
						β	**1.84**	**12.083**

4. Conclusion

The dipole moments of the iodinated coumarin derivatives of 4(3IP)6MC and 4(3IP)6CLC were experimentally determined using polar and nonpolar solvents. For both molecules, the dipole moments in the excited state were found to be substantially greater than those in the ground state. *The μ_e of 4(3IP)6MC* exhibiting values between 7.2 D and 11.3 D, and for 4(3IP)6CLC ranging from 6.7 D to 9.8 D. *Comparative analysis of the dipole moment change ($\Delta\mu$) and the μ_e/μ_g ratio reveals that 4(3IP)6CLC is more favourable, suggesting stronger intramolecular charge transfer upon excitation, leading to a more effective* $\pi \rightarrow \pi^*$ transition. Additionally, solute–solvent interactions were examined using the Kamlet–Taft and Catalán multiple linear regression models, revealing that chlorine substitution in 4(3IP)6CLC enhances polarizability effects and reduces hydrogen-bonding contributions compared to the

4(3IP)6MC. Frontier molecular orbital (HOMO–LUMO) analysis indicates that 4(3IP)6CLC possesses a greater electron-accepting capability, enhanced intramolecular charge transfer, and increased stabilisation in the excited state compared to 4(3IP)6MC. Molecular electrostatic potential (MEP) identifies the electrophilic and nucleophilic regions of molecules, while contour maps illustrate the spatial distribution of electrostatic potential. Furthermore, the nonlinear optical properties demonstrate that 4(3IP)6CLC exhibits a strong response to external electric fields, highlighting its potential as a promising nonlinear optical material for advanced imaging applications.

References

[1]. Mohd Aqib, Khatoon S, *et al.* (2025), Exploring the anticancer potential and mechanisms of action of natural coumarins and isocoumarins, Europiean Journal of medicinal Chemistry Vol. 282., 117088, https://doi.org/10.1016/j.ejmech.2024.117088

[2]. Ljungman M (2009) Targeting the DNA danger response in cancer, Chem. Rev.109, 2929-2950, https://doi.org/10.1021/cr900047g

[3]. Woo Y, Chaurasiya S, O'Leary M, Han E, Fong Y (2021), Fluorescent Imaging for Cancer Therapy and Cancer Gene Therapy, https://doi.org/10.1016/j.omto.2021.06.007

[4]. Makandar S N, Basanagouda M, Kulkarni M V, Pranesha, Rasal V P (2012) Synthesis and antimicrobial studies of some 4-aryloxymethyl coumarins obtained by reaction of 4-bromomethyl coumarins with aromatic bidental enucleophiles, Med.chem.Res 21, 2603-2614, https://doi.org/10.1007/s00044-011-9785

[5]. Basanagouda M, Kulkarni M V, Sharma D, Gupta V K, Pranesha, Sandhya Rani P S, Rasal V P (2009) Synthesis of some new 4-aryloxymethyl coumarins and examination of their antibacterial and antifungal activitiez, J. Chem. Sci., Vol 121, pp 485-495. https://doi.org/10.1007/s12039-009-0058

[6]. Basanagouda M, Jambagi V B, Barigidad N N, Laxmeshwar S S, Devaru V, Narayanachar (2014) Synthesis, structure-activity relationship of iodinated-4aryloxymethyl-coumarins as potential anti-cancer and anti-mycobacterial agents, Eur. J. Med. Chem., Vol 74, pp 225-233. https://doi.org/10.1016/j.ejmech.2013.12.06

[7]. Lakowicz J R (1983) Principle of Fluorescence Spectroscopy, Plenum Press, New York,.

[8]. Lippert E, Naturforsch Z,(1955) Dipole moment und Elektronenstruktur von angeregten Molekülen,10, 541–545.DOI: 10.1515/zna-1955-0707 (1955) 1-5

[9]. Bakshiev N G (1964) *Universal intermolecular interactions and their effect on the position of the electronic spectra of molecules in two-component solutions*, *Optics and Spectroscopy* 16, 821–832,

[10]. Chamma A, Viallet P (1970) Determination of the dipole moment of a molecule in a singlet excited state. C R Acad Sci Paris Ser C 270:1901–1904

[11]. Bilot A K, Kawski A (1962). Z Naturforsch A 17A:621–627. https://doi.org/10.1515/zna-1962-0713

[12]. Reichardt C (1988) Solvents and Solvent Effects in Organic Chemistry. Verlag Chemie, Weinheim, New York

[13]. Taft R W, Abboud JL M, Kamlet M J, Abraham M H (1985) Linear solvation energy relationships. J Solution Chem. 14:153–186. https://doi.org/10.
1007/BF00647061

[14]. Catalán J (2009) Toward a generalized treatment of the solvent effect based on four empirical scales: dipolarity (SdP, a new scale), polarizability (SP), acidity (SA), and basicity (SB) of the medium. The Journal of Physical Chemistry B 113(17):5951–5960. https://doi.org /10.1021/jp8095727

[15]. Robb M A (1916) New chemistry with Gaussian 16 and Gauss View 6. Accessed 25 Sept 2022.

[16]. Zaier R, Ayachi S (2021) Computational study on optoelectronic properties of donor–acceptor type small π-conjugated molecules for organic light-emitting diodes (OLEDs) and nonlinear optical (NLO) applications. In: Density Functional Theory - Recent Advances, New Perspectives and Applications.

[17]. Mahantesha Basanagouda, Vishwanath B. Jambagi, Nivedita N. et.al (2014) Synthesis, structure activity relationship of iodinated-4- aryl oxymethyl-coumarins as potential anti-cancer and antimycobacterial agents, European Journal of Medicinal Chemistry 74 (2014) 225 e233 , http://www.elsevier.com/locate/ejmech

[18]. Nagachandra K H, Mannekutla J R, Amarayya S M, Inamdar S R (2012) Solvent effect on the spectral properties of dipolar laser dyes: Evaluation of ground and excited state dipole moments. European

Journal of Chemistry 3(2):163–171. https://doi.org/10.5155/eurjchem.3.2.163.538

[19]. Wari M N, Inamdar S R (2017) Solvatochromic study of organic dyes: A qualitative approach using semi empirical (ZINDO-IEFPCM) method. International Journal of Pure and Applied Research in Physics 4(1):51–56. ISSN 2455-474X.

[20]. Thipperudrappa J, Deepa H R, Raghavendra U P, Hanagodimath S M, Melavanki R M (2016) Effect of solvents, solvent mixture and silver nanoparticles on photophysical properties of a ketocyanine dye. Luminescence. https://doi.org/10.1002/bio.3147

[21]. Mathapati G B, Ingalagondi P K, et al (2019) Estimation of ground and excited state dipole moments of newly synthesized coumarin molecule by solvatochromic method and Gaussian software. International Journal of Scientific Research in Physics and Applied Sciences 7(2):3843. https://doi.org/10.26438/ijsrpas/v7i2.3843

[22]. Devar S, More S, Patil O, Nagesh G Y, Hanagodimath S M (2025) Synthesis, spectroscopic, DFT calculation and molecular docking studies of indole derivative. Journal of Fluorescence. https://doi.org/10.1007/s10895-025-04301-2

[23]. More S, Patil O, Devar S, Hanagodimath S M (2024) Estimation of electric dipole moment by solvatochromism, computational method, and study of the effect of solvents by preferential solvation of 6-methoxy-4-(4-nitrophenoxy methyl)-chromen-2-one (6MNPM). Journal of Fluorescence. https://doi.org/10.1007/s10895-024-03955-8

[24]. Edward J T (1956) Molecular volumes and parachor. Chemistry and Industry (London) 774.

[25]. Ravi M, Samanta A, Radhakrishnan TP (1995). Journal of the Chemical Society, Faraday Transactions 91:2739. https://doi.org/10.1039/FT9959102739

[26]. Reichardt C (1994) Solvatochromic dyes as solvent polarity indicators. Chemical Reviews 94(8):2319–2358. https://doi.org/10.1021/cr00032a005.

[27]. Waghorne, W.E., 2024. Solvent acidity and basicity scales: Analysis of Catalan's SB and SA scales and comparison with Kamlet–Taft β and α scales. *J. Solution Chem.* 53, 747–760. https://doi.org/10.1007/s10953-024-01382-8.

[28]. Homocianu, M., et al., 2023. Solvatochromism correlated with Kamlet–Taft and Catalán solvent scales. *Int. J. Mol. Sci.* 24, 5286. https://doi.org/10.3390/ijms24065286.

[29]. Parr R G, Szentpály L V, Liu S (1999) Electrophilicity index. Journal of the American Chemical Society 121(9):1924–1932. https://doi.org/10.1021/ja983494x.

[30]. More S, Patil O, Chillargikar S, Lalasangi D, Hanagodimath S M (2025) DFT-based quantum chemical analysis of coumarin derivatives. The Nucleus 62(1):37–46. https://doi.org/10.71330/thenucleus.2025.1445.

[31]. Devar S, More S, Patil O, Nagesh G Y, Hanagodimath S M (2023) Quantum chemical calculation and molecular docking studies of indole derivative. European Chemical Bulletin 12(Special Issue 5):6704–6717. https://doi.org/10.48047/ecb/2023.12.si5a.0603.

[32]. Basavaraj S, Gonnalli S, Patil O, Hanagodimath S M (2021) Quenching of fluorescence, dipole moments and DFT studies of newly synthesized amino-thiadiazole coumarin derivative. Journal of the Maharaja Sayajirao University of Baroda 55(1). ISSN 0025-0422

[33]. Ayachit N H (2010) Excited state electric dipole moments of two laser dyes from solvatochromic shifts. Journal of Electron Spectroscopy and Related Phenomena 180:14–16. https://doi.org/10.1016/j.elspec.2010.01.004

[34]. Shashirekha V, Umadevi M, Ramakrishnan V (2008) Solvatochromic study of 1,2-dihydroxyanthraquinone in neat and binary solvent mixtures. Spectrochimica Acta Part A: Molecular and Biomolecular Spectroscopy 69:148 https://doi.org/10.1016/j.saa.2007.03.021

[35]. Tsague L F, Ejuh G W, Teyou Ngoupo A, Tadjouteu Assatse Y, Yossa Kamsi R A, Ottou Abe M T, Ndjaka J M B (2023) Ab-initio and density functional theory (DFT) computational study of the effect of fluorine on the electronic, optical, thermodynamic, hole and electron transport properties of the circumanthracene molecule. Heliyon 9:e19647. https://doi.org/10.1016/j.heliyon.2023.e19647

[36]. Patil O, Ingalagondi P K, Mathapati G B, Hanagodimath S M (2018) Estimation of ground and excited state dipole moments of newly synthesized coumarin (4-MPMHC) derivative. JETIR 5(9).

[37]. Shivaleela B, Hanagodimath S M (2020) Ground state and excited state dipole moments of coumarin derivative 4ATMC. In: *Proceedings of the International Conference on Advanced Materials*, pp 240–248.

[38]. J.Tipperudrappa, U.P.Raghavendra, Mahantesh Basanagouda (2014) Photophysical characteristics of biologically active 4-aryloxymethyl coumarin 4PTMBC and 1IPMBC, Spectrochim Acta A Mol Biomol Spectrosc . DOI: 10.1016/j.saa.2014.10.039

[39]. Chandrasekhar, S.; Deepa, H. R.; Melavanki, R. M.; Mogurampelly, S.; Basanagouda, M. M.; Yallappa, S.; Thipperudrappa, J. "*Quantum chemical and solvatochromic studies of biologically active 1,3,4-thiadiazol coumarin derivatives*". Chemical Data Collections 2020, *29*, 100516. https://doi.org/10.1016/j.cdc.2020.100516

[40]. Shivaleela B, Shivaraj G G, Hanagodimath S M (2023) Estimation of dipole moments by solvatochromic shift method, spectroscopic analysis of UV–visible, HOMO–LUMO, ESP map, Mulliken atomic charges, NBO, NLO properties of benzofuran derivative. Results in Chemistry 6:101046. https://doi.org/10.1016/j.rechem.2023.101046

[41]. Gonnalli S G, Basavaraj S, Hanagodimath S M Spectroscopic analysis of NMR, IR, UV–Vis, HOMO–LUMO, ESP and Mulliken charges of coumarin derivatives by density functional theory. Journal of the Maharaja Sayajirao University of Baroda. ISSN 0025-0422.

[42]. Choudhary V K, Bhatt A K, Dash D, Sharma N (2019) DFT calculations on molecular structure, HOMO–LUMO study, reactivity descriptions and spectral analysis of newly synthesized diorganotin(I V) 2-chloridophen
ylacetohydroxamate complexes. Journal of Computational Chemistry 40(27):2354–2363. https://doi.org/10.1002/jcc.26012

[43]. Jayarajan R, Satheeshkumar R, Kottha T, Subbaramanian S, Sayin K, Vasuki G (2020) Water mediated synthesis of 6-amino-5-cyano-2-oxo-N-(pyridin-2-yl)-4-(p-tolyl)-2H-[1,2'-bipyridine]-3-carboxamide and 6-amino-5-cyano-4-(4-fluorophenyl)-2-oxo-N-(pyridin-2-yl)-2H-[1,2'-bipyridine]-3-carboxamide – An experimental and computational studies with nonlinear optical (NLO) and molecular docking analyses. Spectrochimica Acta Part A: Molecular and Bimolecular Spectroscopy 229:117861. https://doi.org/10.1016/j.saa.2019.117861.

[44]. Balachandar Waddar, Suman Gandi, S. R. Parne, V. R. Chari, G. R. Prasanth (2024) Investigation of Second-Order NLO Properties of Novel 1,3,4-Oxadiazole Derivatives: A DFT Study (2024) Journal of Molecular Modeling, Vol 30, Article 118 DOI: 10.1007/s00894-024-05910-7